PROCEEDINGS REPRINT

EUROPTO SERIES

Reprinted from

Optics in Atmospheric Propagation and Adaptive Systems

27–28 September 1995
Paris, France

Volume 2580

Modeling for atmospheric background radiance structures

John Gruninger, Robert L. Sundberg, and James W. Duff
Spectral Sciences, Inc., Burlington, MA

James Brown and Ramesh Sharma
USAF Phillips Laboratory/GPOS, Hanscom AFB, MA

Robert D. Sears
Jamieson Science and Engineering, Albuquerque, NM

ABSTRACT

Atmospheric infrared radiance fluctuations result from fluctuations in the density of atmospheric species, individual molecular state populations, and kinetic temperatures and pressures along the sensor line of sight (LOS). The SHARC-4 program models the atmospheric background radiance fluctuations. It predicts a two dimensional radiance spatial covariance function from the underlying 3D atmospheric structures. The radiance statistics are non-stationary and are dependent on bandpass, sensor location and field of view (FOV). In the upper atmosphere non-equilibrium effects are important. Fluctuations in kinetic temperature can result in correlated or anti-correlated fluctuations in vibrational state temperatures. The model accounts for these effects and predicts spatial covariance functions for molecular state number densities and vibrational temperatures. SHARC predicts the the non-equilibrium dependence of molecular state number density fluctuations on kinetic temperature and density fluctuations, and calculates mean LOS radiances and radiance derivatives. The modeling capabilities are illustrated with sample predictions of MSX like experiments with MSX sensor bandpasses, sensor locations and FOV. The model can be applied for all altitudes and arbitrary sensor FOV including nadir and limb viewing.

1. INTRODUCTION

The calculation of infrared (IR) mean radiance, transmittance and their fluctuation statistics is important in many areas of atmospheric science, including the interpretation of satellite sensor measurements and for understanding the effects of turbulence structures on molecular excitation processes. The atmospheric infrared radiance fluctuations depend on fluctuations in atmospheric species number densities, vibrational state populations, and the kinetic temperatures along the sensor line-of-sight (LOS). The standard SHARC model[1] calculates mean LOS radiance and transmittance values. The SHARC structure model predicts the two-dimensional spatial covariance function of the radiance. The covariance function and its Fourier transform, the power spectral density (PSD), can be use directly in sensor models or in image synthesis modes to create realizations of the predicted structure. The radiance statistics and images are non-stationary and are explicitly bandpass and sensor FOV dependent.

At lower altitudes (~50 km), collisional quenching of excited vibrational states is fast compared to radiative decay. Species tend to be in local thermodynamic equilibrium (LTE) and state populations can be determined from a Boltzmann distribution at the gas-kinetic temperature. At higher altitudes, there are an insufficient number of collisions to equilibrate vibrational energy before radiative decay occurs and the vibrational states can no longer be characterized by the kinetic temperature. Under these conditions, the vibrational states are in nonlocal thermodynamic equilibrium (NLTE). Models extending into the higher altitudes must describe these deviations from local thermodynamic equilibrium. SHARC assumes steady state kinetics for the atmospheric processes of collisional excitation, energy transfer, radiative decay, chemical production and illumination by the sun, earth and atmosphere. The model includes seven species which radiate in the 2-40 μm wavelength region. It includes NO, CO_2, O_3, H_2O, OH, CO, and CH_4. Isotopes of CO_2 and H_2O are also modeled. The number densities of the excited vibrational states are predicted and can be described in terms of a Boltzmann distribution with state dependent vibrational temperatures. Under LTE conditions, the responses to a kinetic temperature fluctuation can be described by a Boltzmann distribution corresponding to the new kinetic temperature. The emission from a small volume in the atmosphere depends only on the gas-kinetic temperature in that volume and is determined using the Planck blackbody emission source term at the new fluctuated temperature. Under NLTE conditions, the response of population changes to fluctuations in temperature and density are determined for each state by a perturbation model which uses the same steady state chemical-kinetics schemes that are used for the quiescent atmosphere. Fluctuations in the kinetic temperature can result in correlated or anti-correlated responses in vibrational state population. The magnitudes of the responses depend on the local chemical environment. NLTE emission depends on the vibrational temperatures of all species involved, as well as, the gas-kinetic temperature.

0-8194-1944-3/95/$6.00

Fluctuations in atmospheric temperature and density have been measured directly using balloon, rocket, and satellite experiments. These experiments provide in-situ measurement of density, temperature and species concentrations. Ground based techniques used to determine atmospheric structure statistics include radar, lidar and airglow emission measurements. Taken together these measurements begin to provide the necessary structure statistics which characterize the atmosphere. Current estimates of these quantities have been summarized, in a 3-D non-stationary statistical model (NSS).[2] The NSS model provides a covariance function, PSD description of atmospheric temperature and density fluctuations. Horizontal altitude layers are assumed to be isotropic and stationary. The vertical variations are non-stationary. Model parameters (variance, vertical correlation length, and horizontal correlation length) are described as a function of altitude. The NSS model currently assumes a 1-D PSD spectral slope of -2 for all altitudes.

A simulation of the radiance fluctuations observed by a sensor array can be calculated by using a three-dimensional realization of the atmospheric temperature and density fluctuations and by intersecting a LOS for each pixel with the 3-D realization to determine the LOS radiance for each pixel in the sensor.[3] Alternatively, the radiance statistics for the sensor FOV can be derived directly. The radiance statistical functions can be incorporated into sensor models, or image syntheses models, to create realizations of the radiance statistics. The model described here proceeds with the later approach although the former approach is being used to evaluate the algorithms. The radiance statistics predicted by SHARC explicitly include radiance fluctuation contributions along the entire LOS and not just the tangent point. The inputs to the calculation are altitude dependent temperature and density profiles, which can be obtained from the standard atmosphere generator code (SAG),[4] the local temperature and density statistical quantities obtained form the NSS model and an atlas of molecular line parameters based on HITRAN-92.[5] The SHARC model calculates the non-stationary LOS radiance covariance by performing LOS integrations over the products of radiance fluctuation amplitude functions,[6] and the local kinetic temperature covariance. A key quantity derived by the model is a LOS radiance variance distribution function which determines the contribution to radiance variance of each portion of the LOS. The radiance variance distribution function act as a weighting function. It reveals contributions of temperature and density fluctuations to radiance variance along the LOS.

2. RADIANCE STRUCTURE CALCULATION TECHNIQUE

The radiance structure of atmospheric backgrounds is induced by local temperature and density fluctuations in the atmosphere. The radiance in a pixel of an image plane $L_{\Delta\lambda}(\vec{p})$, is given by

$$L_{\Delta\lambda}(\vec{p}) = \int d\lambda \int dr \; S(\vec{r},\lambda)\partial\tau(r,\lambda)/\partial r \quad . \tag{1}$$

The quantity $S(\vec{r},\lambda)$ is the emission source term at the wavelength, λ. The atmospheric transmittance, τ, along the LOS depends on the scalar distance r from the observer to the pixel and $\vec{p}$ is a vector in the sensor plane defining the pixel location. In the LTE approximation the source term is the Plank blackbody function at the local atmospheric gas kinetic temperature, T_k. In The NLTE regime the source term is dependent on the non-equilibrium number densities of the molecular states involved in the bandpass.[1] The populations of rotational states involved in the the bandpass transitions are assumed to be in LTE. The vibrational states, j, are in NLTE. The dependence can be expressed in terms of vibrational state temperatures, T^j_{vib}. Implicit in Equation (1) is a sum over all species and there molecular states which emit in the bandpass, $\Delta\lambda$.

2.1 Vibrational state temperature fluctuations

The local temperature and density fluctuations specified in the NSS model induce fluctuations in the local vibrational state number densities. The influence of temperature and density enter into the chemical kinetic rate equations in a non-linear fashion. The collision rates are affected by temperature variations which alter rate constants and density variations which influence the number of collisions. The model predicts fluctuations in local vibrational state densities as a function of local temperature and density fluctuations. Temperature fluctuations cause two effects, a simple expansion or compression which changes state populations induced by local heating or cooling respectively, and the adjustment of vibrational/rotational state populations due to chemical kinetic mechanism. The latter effect can be expressed in terms of fluctuations in vibrational and rotational state temperatures. In this work, the rotational states are considered to be LTE, so rotational temperatures and fluctuations map exactly with kinetic temperature fluctuations.

The fluctuation in local vibrational temperature for a specified vibrational state, j, can be approximated as

$$\Delta T^{j}_{vib} = (\partial T^{j}_{vib}/\partial T_{k})\Delta T_{k} + \ldots \quad (2)$$

The proportionality constants, $(\partial T^{j}_{vib}/\partial T_{k})$, are strongly dependent on altitude and are also far from the LTE value of unity when NLTE effects are important.

As an example we illustrate the results of the NLTE kinetics model for determining the nighttime estimates of vibrational temperature and its response to temperature fluctuations for the CO_2 ν_2 and ν_3 fundamental transitions, see Figures 1 and 2. NLTE effects in vibrational state populations, and their linear response to fluctuations in temperature and occurs for these states above 40 to 50 km. The NLTE effects in vibrational temperature is consistent with previous NLTE models and has been presented previously.[1] Although vibrational temperature fluctuations have not been examined by other models, the fluctuations can be understood in terms of the same atmospheric processes determining the vibrational temperatures. In particular, the $CO_2(\nu_2)$ vibrational state involves collisional excitation by N_2 and O_2 which is dominates below 50 km in the LTE regime, and diminishes in importance above 100 km. Radiative pumping in important above 50 km and dominates between 80 km and 100 km corresponding to the minimum in $\partial T_{vib}/\partial T_{k}$ around 80 km, as shown in Figure 2. Above 90 km, O atom excitation becomes increasingly important until ~250 km where again radiative excitation dominates. The behavior of the $CO_2(\nu_3)$ state is quite different than $CO_2(\nu_2)$. $CO_2(\nu_3)$ is LTE up to approximately 30 km, and becomes completely dominated by radiative excitation by 50 km up to an altitude of 100 km. Although vibrational-to-vibrational energy transfer between CO_2 and N_2 is an the most important mechanism between 110 and 170, there are not sufficient collisions to provide significant variations in the vibrational temperature in this altitude regime. Clearly, the altitude variations of the vibrational temperatures in response to temperature fluctuations will have a profound effect on the radiance fluctuations.

2.2 Radiance covariance

A fluctuation in radiance is approximated using the lead terms of a Taylor series expansion in terms of the vibrational state temperatures and the atmospheric temperature.

$$\Delta L_{\Delta\lambda}(\vec{p}) = \int dz\{\sum_{j} F^{j}_{\Delta\lambda}(\vec{r})\Delta T^{j}_{vib} + F^{0}_{\Delta\lambda}(\vec{r})\Delta T_{k}\} + O[(\Delta T_{k})^{2}] \quad . \quad (3)$$

The $F^{j}_{\Delta\lambda}$ and $F^{0}_{\Delta\lambda}$ are local LOS fluctuation amplitude functions. The radiance fluctuations induced by the rearrangement of population among the molecular vibrational states, j, is given by

$$F^{j}_{\Delta\lambda}(\vec{r}) = \int d\lambda \partial[S\vec{r},\lambda)\partial\tau(r,\lambda)/\partial r]/\partial T^{j}_{vib} \quad . \quad (4)$$

The radiance fluctuation induced by population shifts among rotational states, which are assumed to be in LTE, and the expansion or compression of the gas is given by

$$F^{0}_{\Delta\lambda}(\vec{r}) = \int d\lambda \ \partial[S\vec{r},\lambda)\partial\tau(r,\lambda)/\partial r]/\partial T_{k} \quad . \quad (5)$$

Only the linear terms in Equations (2) and (3) are retained to make a direct estimate of the radiance statistics.[7] This approach is an extension of an LTE approximation used to determine atmospheric radiance statistics.[6] The expression for a radiance fluctuation can be simplified in the linear approximation to

$$\Delta L_{\Delta\lambda}(\vec{p}) = \int dr\ F_{\Delta\lambda}(\vec{r})\Delta T_k \quad , \tag{6}$$

where $F_{\Delta\lambda}(\vec{r})$ includes radiance fluctuation contributions from both vibrational state temperature fluctuations and kinetic temperature fluctuations.

$$F_{\Delta\lambda}(\vec{r}) = \sum_j F^j_{\Delta\lambda}(\vec{r})\partial T^j_{vib}/\partial T_k + F^0_{\Delta\lambda}(\vec{r}) \quad . \tag{7}$$

The fluctuation amplitude is a linear response model for radiance fluctuations in terms of gas kinetic temperature fluctuations. This model can be coupled with a statistical model for non-stationary atmospheric temperature fluctuations to obtain a statistical non-stationary description of radiance fluctuations. In this work we use the NSS[2] model.

The radiance covariance $Cov_L(\vec{p}_1,\vec{p}_2)$, where $\vec{p}_1$ corresponds to point 1, and $\vec{p}$ to point 2, in the sensor plane, can be expressed as

$$Cov_L(\vec{p}_1\vec{p}_2) = E[\Delta L_{\Delta\lambda}(\vec{p}_1)\Delta L_{\Delta\lambda}(\vec{p}_2)] \quad , \tag{8}$$

where E is the expectation value, as illustrated in Figure 3. Substituting Equation (6) into Equation (8) yields

$$Cov_L(\vec{p}_1\vec{p}_2) = \int dr_1 \int dr_2 F_{\Delta\lambda}(\vec{r}_1)F_{\Delta\lambda}(\vec{r}_2)Cov_T(\vec{r}_1,\vec{r}_2) \quad . \tag{9}$$

The radiance variance, $\sigma^2_L(\vec{p})$, is determined by setting $\vec{p}_1 = \vec{p}_2$ in Equation (9) so there is zero lag

$$\sigma^2_L(\vec{p}) = \int dr \int dr' F_{\Delta\lambda}(\vec{r})F_{\Delta\lambda}(\vec{r}')Cov_T(\vec{r},\vec{r}') \quad . \tag{10}$$

Equation (10) shows dependence of the radiance variance on the atmospheric temperature covariance along the LOS direction. Integration over one of the variables in Equation (10) leads to a LOS variance distribution function, or weighting function, $w_{\Delta\lambda}(\vec{r})$,

$$\sigma^2_L(\vec{p}) = \int dr\ w_{\Delta\lambda}(\vec{r}) \tag{11}$$

where

$$w_{\Delta\lambda}(\vec{r}) = \int dr' \, F(\vec{r})F(\vec{r})Cov_T(\vec{r},\vec{r}) \quad . \tag{12}$$

The variance distribution function determines how contributions to the radiance structure are distributed along the LOS through the atmosphere. The area under the distribution curve is the radiance variance at the the pixel location $\vec{p}$. The variance distribution function, $w_{\Delta\lambda}$, can be evaluated numerically or it can be estimated by an approximation suggested by Lindquist, Kwon, and Nagy.[8] If the radiance fluctuation amplitude is a slowly varying function of location along the LOS, the product $F(\vec{r}_1)F(\vec{r}_2)$ can be replaced by the product of the radiance fluctuation amplitudes, $F(\vec{r})$,[2] at the midpoint location, $\vec{r}$, and taken outside of the integral. The integral of the temperature covariance function yields the temperature correlation length along the LOS direction.

$$w_{\Delta\lambda}(\vec{r}) = F_{\Delta\lambda}(\vec{r})^2 \, l_r(\vec{r}) \quad . \tag{13}$$

For this approximation to be valid, the local bandpass LOS weighting functions, F, must be slowly varying over the range of a temperature correlation length. Current estimates for the LOS weighting function are slowly varying compared to LOS temperature correlation lengths estimated using the NSS model. As a second test of Eq. (13), numerical integration of Eq. (12) using assumed functional forms for the temperature covariance suggest that the integral is independent of the functional form of the covariance and provides results within a few percent of Eq. (13). The covariance weighting functions, $w_{\Delta\lambda}$, is evaluated numerically by SHARC. The role of the spatial statistics of the 3-D temperature structures is revealed through the radiance variance distribution function. The temperature correlation length along the LOS direction controls the extent to which temperature fluctuations are averaged by LOS radiation transport. The temperature correlation lengths perpendicular to the LOS determine the spatial radiance statistics in the sensor plane. The statistical properties of the radiance fluctuations such as correlation angles or lengths can be determined directly from the covariance function, or they can be approximated using the variance distribution function.[7]

2.3 Image synthesis

The bandpass dependent statistics of the radiance fluctuations, can be input into a model for synthesizing images. The radiance statistics are non-stationary. This requires an image generator which can deal with spatially varying statistics. In this effort we utilize the Poorman's Image Generator (PIG),[6] which was developed for the purpose of rapid generation of non-stationary statistical structures. Input to PIG are the mean radiance, horizontal and vertical correlation lengths, and a variance for each altitude. The model uses Fourier techniques to generate horizontal correlations and an auto-regressive (AR) method to synthesize vertical non-stationary correlations.

First, the image is correlated in the stationary direction. In the Fourier approach a zero mean, unit variance Gaussian random image is transformed and each scan line is filtered by a Power Spectral Density (PSD). The PSD corresponds to an assumed power spectra for the altitude or to a numerical spectra determined from the radiance covariance. The image is then inverse transformed. The horizontally correlated image is then correlated in the vertical direction using the AR approach. In the non-stationary direction, the vertical correlation function is assumed to be exponential, leading to a single AR parameter.[9] This exponential assumption allows a rapid algorithm, but is not always representative of vertical covariance functions. More accurate methods are currently being developed.

3. RADIANCE STRUCTURE STATISTICS AND IMAGES

The model described in this paper has been applied to calculate the radiance structure for two bands under nighttime conditions. One of the bandpasses samples radiance from $CO_2(v_3)$, MSX band B1, the second bandpass samples radiance from the fundamental $NO(\Delta v=1)$ and $O_3(v_3)$ bands, MSX band A. The predicted variance weighting functions for the day and night CO_2 (v_3) are illustrated in Figures 4 and 5. They are given as a function of altitude from the upper atmosphere to the limb. Because of the opacity found in this bandpass, the emission from the later half of the LOS does not reach the observer and plays no role in the radiance statistics. There are strong diurnal effects with the day mean radiance being two orders of magnitude larger than the night radiance, above about 60 km.

Solar pumping of the CO_2 hot bands is responsible for this difference below 90 km where the fundamental is essentially self absorbed. The magnitude of the variance distribution function determines the extent to which a particular portion of the atmosphere contributes to the radiance structure at the sensor. Strong absorption at approximately 40 km causes structure at this altitude to contribute to all tangent point altitudes below, for both day and night. Solar pumping effects the magnitudes of daytime mean radiance and the variance distribution function. There are knees in the nighttime and daytime weighting function at 120 km, 90 km and 45 km and a small daytime knee at 70 km. The effect of these knees is that the local atmospheric structure at the knee altitudes strongly affect the structure along the LOS with lower tangent point altitudes. For example, the 120 km knee causes the structure in LOS with tangent points between 90 and 120 to be dominated by the structure at 120 km. The nighttime knee is larger and therefore has a greater effect on the structure parameters. Likewise the strength of the daytime knee at 90 km and the existence of a small knee at 70 km significantly influence the LOS penetrating to lower altitudes, in fact all the way down to the next knee at 45 km.

The radiance statistics at the sensor can be compared to the temperature statistics at the tangent point altitude by projecting the radiance values to the tangent point range. This corresponds to converting a distance in the image plane to the corresponding distance at the tangent point (see Figure 3). The resulting radiance correlation lengths at the tangent point are shown in Figures 6 and 7. They track the temperature correlation lengths above 120 km (not shown), but below the knees in the radiance distribution function, the statistics are determined by the higher altitudes. This behavior results from dominance of the high altitude part of the LOS variance function for LOS paths which are below the knees in the variance distribution function, as shown in Figures 4 and 5. The magnitude of the knee determines the extent of the effect on the lower altitudes, thus leading to diurnal effects in the spatial structure. The calculated mean radiances and variances are illustrated in Figure 8. The relative variances, the absolute variances divided by the absolute mean radiance, as a function of altitude are illustrated in Figure 9. The relative variances are typically insensitive to small changes in the band edges and is typical for all $CO_2(\nu_3)$ band passes. While the mean radiance during the day is two orders of of magnitude larger during the day, the larger relative variances together with the shorter correlation lengths at the lower altitudes, would give the night radiance a larger relative gradient structure. Figures 10 and 11 shows image realizations of the resulting day and night radiance statistics for the CO_2 (ν_3) MSX band B1. The dc component of the radiance has been removed to highlight the structure.

The second set of calculations are for the MSX band A, which is optically thin. For optically thin bands, the radiance variance distribution is not effected by self absorption, and the altitude sampling shows no diurnal effects. Typically the largest concentrations of radiative species is at the tangent point and the spatial radiance statistics is dominated by the tangent point temperature statistics. This is the situation with $O_3(\nu_3)$. The day and night correlation lengths predicted for band A, shown in Figures 12 and 13, closely follow the tangent point temperature statistics up to 100 km. Above 100 km, the radiance statistics are influenced by a large knee at 130 km due to strong fluctuations in the NO radiance. These fluctuations are caused by the large component of O atom collisional excitation of the NO fundamental in this altitude range. Solar illumination photodissociates O_3 between 70 and 105 and introduces a diurnal effect in both mean radiance and variance between these altitudes. The calculated mean radiances and variances are illustrated in Figure 14. At tangent altitudes above 100 km NO(Δv=1) dominates the intensity, the $O_3(\nu_3)$ radiance dominates the intensity below 100 km. The relative variance of the band radiance under daytime and nighttime conditions is plotted as a function of tangent point altitude in figure 15. An image realization for the daytime. radiance structure is given in Figure 16. Note the large variations in structure above 100 km.

4. CONCLUSION

The radiance structure of atmospheric backgrounds is induced by local temperature and density fluctuations in the atmosphere. The model used here predicts the 2-D radiance covariance in the image plane of the sensor from a 3-D model of the temperature covariance. The mean radiances and radiance covariances are calculated using non-equilibrium vibrational state distributions. The model includes specific bandpass dependence, observer-target geometry effects, and diurnal effects. At high altitudes NLTE effects are important. These effects must be included in estimating the mean excited state number densities and the changes in number densities induced by temperature fluctuations. Perhaps the most important result of this work is the clear demonstration that the entire LOS path must be included to accurately determine the radiance statistics. The importance of various altitudes along the LOS can be assessed by the variance distribution function.

5. ACKNOWLEDGMENTS

This work sponsored by Ballistic Missile Defense Organization under Air Force Contract No. F19628-91-C-0083. The authors are grateful to Drs. William Blumberg and Laila Jeong (Phillips Laboratory) for continuing support and interest in this work.

6. REFERENCES

1. R. L. Sundberg, J. W. Duff, J. H. Gruninger, L. S. Bernstein, M. W. Matthew, S. M. Adler-Golden, D. C. Robertson, R. D. Sharma, J. H. Brown, and R. J. Healey, "SHARC, A Model for Calculating Atmospheric Infrared Radiation Under Non-Equilibrium Conditions," in The Upper Mesosphere and the Lower Thermosphere: A Review of Experiment and Theory, Geophysical Monograph Series, 87, 287-295, 1995.
2. L. A. Strugala, R. D. Sears, J. E. Newt, and B. J. Herman, "Production of Statistically Nonstationary Stochastic Structure Realizations for Infrared Background Scene Simulations," Optical Engineering, 32, 993-1000, 1993.
3. J. H. Brown, "Synthetic 3-D Atmospheric Temperature Structure: A Model for Known Geophysical Power Spectra Using A Hybrid Autoregression and Fourier Technique," *PL-TR-94-2150 Phillips Laboratory, 29 Randolph Road Hanscom AFB, MA 1721-3010*, May 1994.
4. S. M. Adler-Golden, "Description of the SHARC Atmosphere Generator," *PL-TR-93-2123, Phillips Laboratory, 29 Randolph Road Hanscom AFB, MA 1721-3010*, May 1993.
5. L. S. Rothman, R. R. Gamache, A. Goldman, L. R. Brown, R. A. Toth, H. M. Pickett, R. L. Poynter, J.-M. Flaud, C. Camy-Peyret, A. Barbe, N. Husson, C. P. Rinsland, and M. A. H. Smith, "The HITRAN Molecular Database: Editions of 1991 and 1992," J. Quant. Spectrosc. Radiat. Transfer, 48, 469, 1992.
6. J. H. Gruninger, R. L. Sundberg, and P. De, "A Model For Atmospheric Radiance Clutter With Applications to Advanced BMD Interceptor Scenarios," Proceedings of the IRIS Meeting on Targets, Backgrounds, and Discrimination, February 1994.
7. R. L. Sundberg, J. H. Gruninger, and J. H. Brown, "Infrared Radiance Fluctuations in the upper Atmosphere", SPIE Proceedings of the International Symposium on Optical Engineering in Aerospace Sensing, 2223, Orlando FL, April 1994.
8. G. H. Lindquist, H. Kwon, and A. R. Nagy, Jr., "Model for Atmospheric Clutter as Seen From a Satellite Platform". Proceedings of the Infrared Technology Conference, SPIE, 430, 24-31, 1983.
9. S. L. Marple, Jr., *Digital Spectral Analysis with Applications*, Prentice-Hall, NJ, 1987.

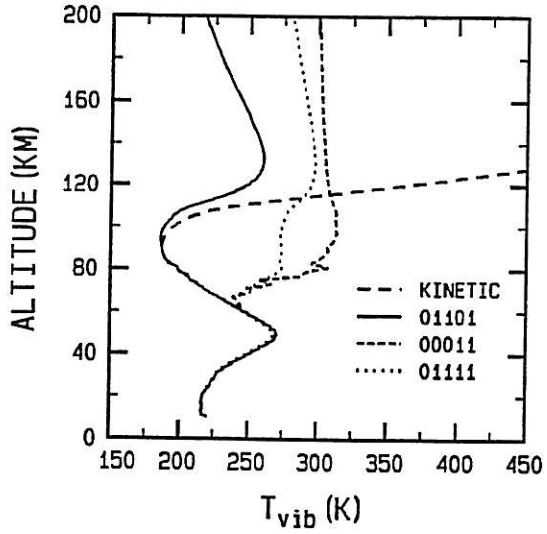

Figure 1. Atmospheric profile kinetic temperature and vibrational temperatures of selected states of CO_2 for nighttime conditions plotted as a function of altitude.

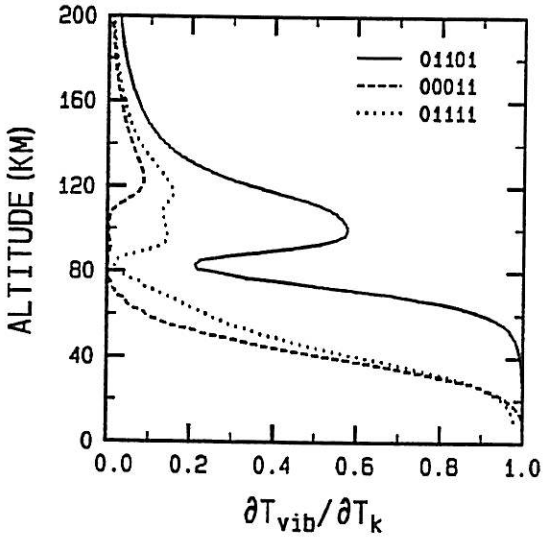

Figure 2. Partial derivatives of vibrational temperature with respect to kinetic temperature as a function of altitude for selected states of CO_2 for nighttime conditions.

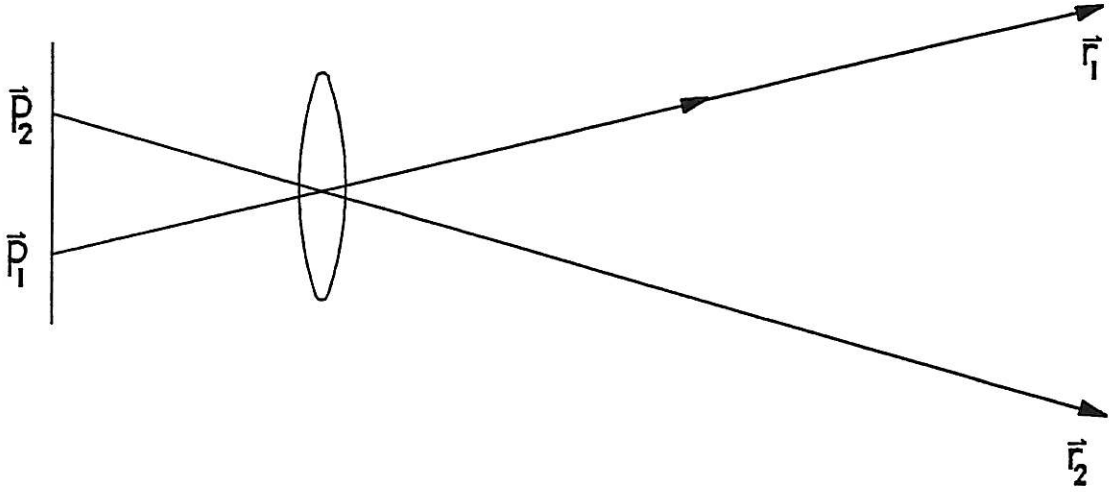

Figure 3. Cartoon of sensor image plane, optics, and two LOS extending into the atmosphere.

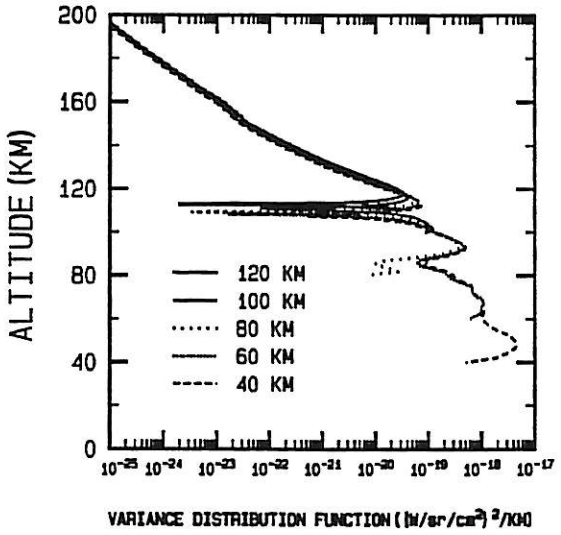

Figure 4. LOS variance distribution functions for daytime limb in the $CO_2(\nu_3)$ band plotted as functions of altitude.

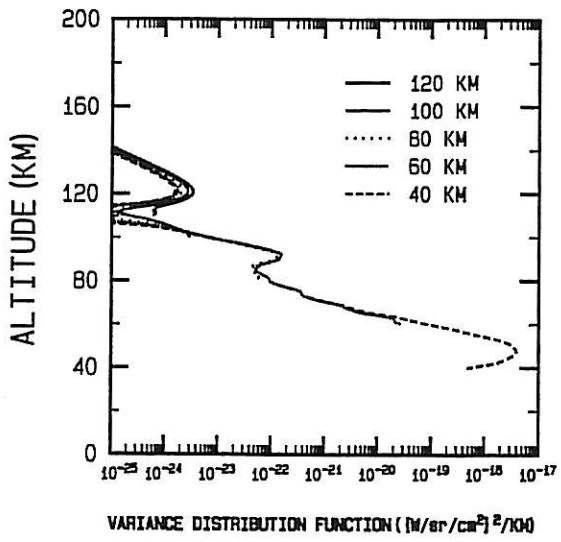

Figure 5. LOS variance distribution functions for nighttime limb in the $CO_2(\nu_3)$ band plotted as functions of altitude.

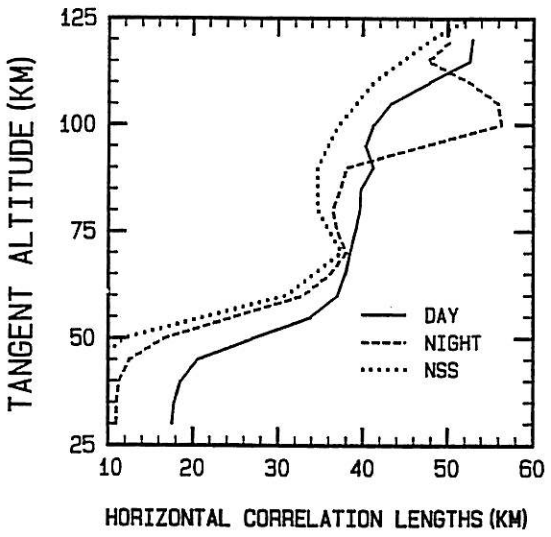

Figure 6. Horizontal radiance correlation lengths plotted as a function of LOS tangent altitude for $CO_2(\nu_3)$ band for daytime and nighttime conditions and an observer at 900 km altitude. The horizontal atmospheric temperature correlation lengths of the NSS input model are also plotted for comparison.

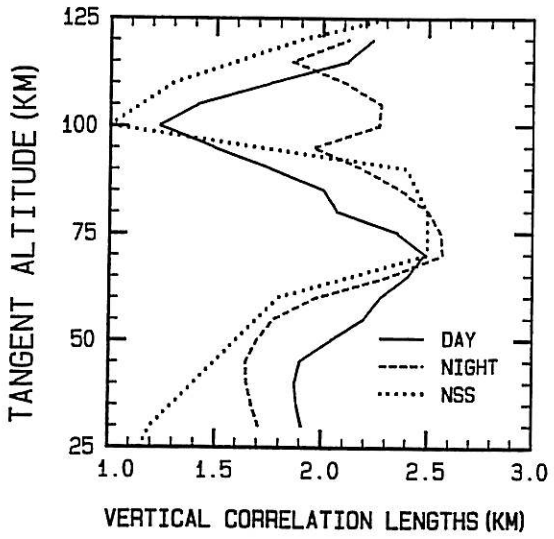

Figure 7. Vertical radiance correlation lengths plotted as a function of LOS tangent altitude for $CO_2(\nu_3)$ band for daytime and nighttime conditions and an observer at 900 km altitude. The vertical atmospheric temperature correlation lengths of the NSS input model are also plotted for comparison.

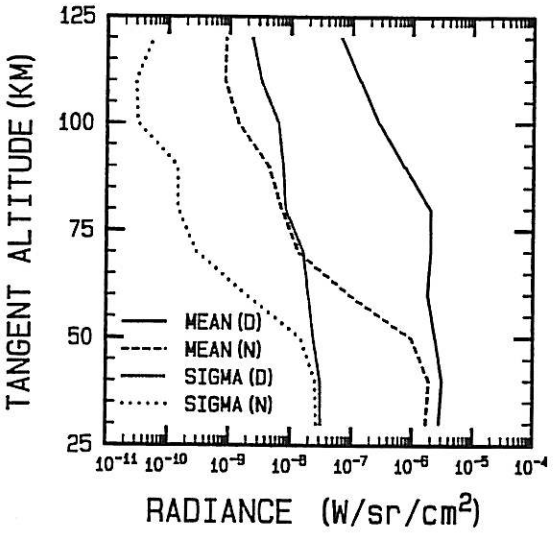

Figure 8. Mean radiances and variances, of the $CO_2(\nu_3)$ band radiance for daytime and nighttime conditions as a function of tangent point altitude.

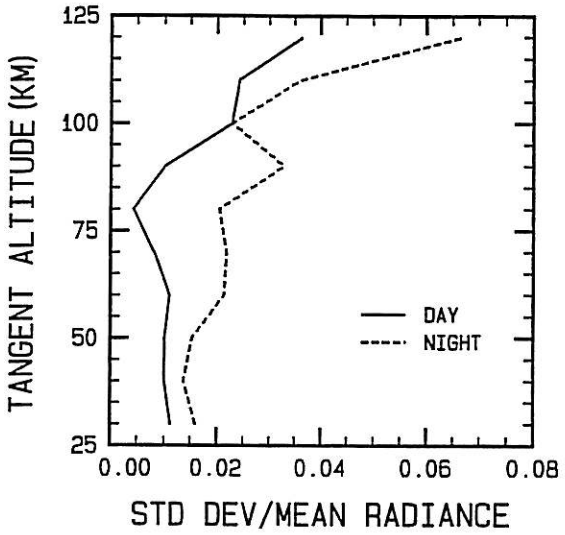

Figure 9. Relative variances, of the $CO_2(\nu_3)$ band radiance for daytime and nighttime conditions.

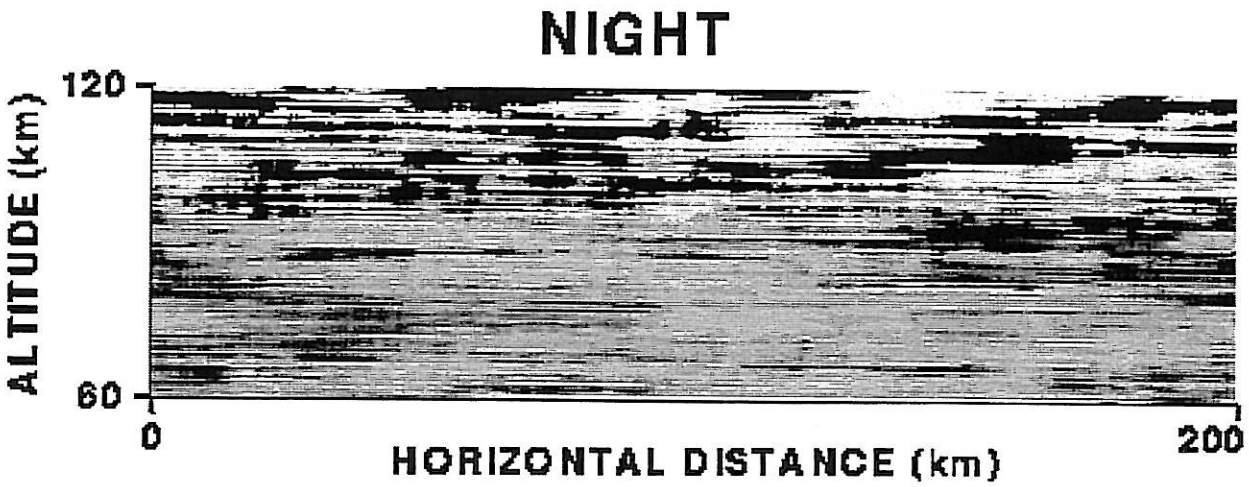

Figure 10. Image of radiance structure in the $CO_2(\nu_3)$ band for nighttime conditions.

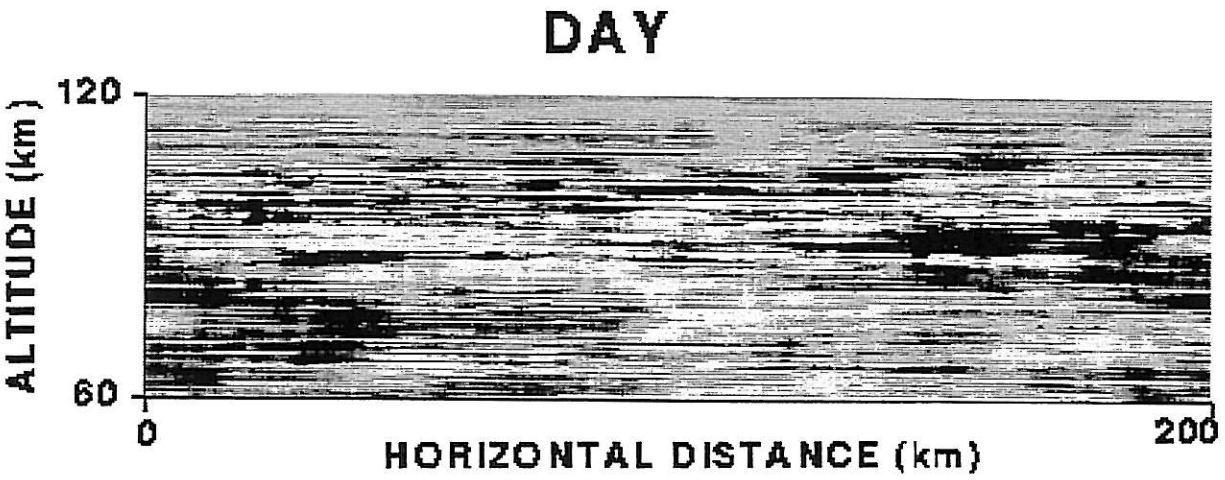

Figure 11. Image of radiance structure in the $CO_2(\nu_3)$ band for daytime conditions.

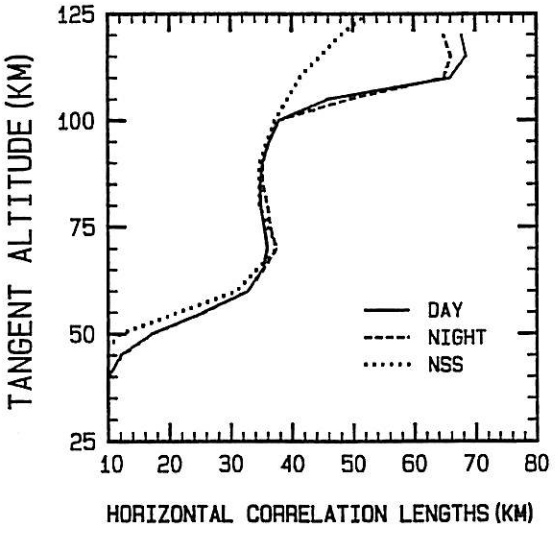

Figure 12. Horizontal radiance correlation lengths plotted as a function of LOS tangent altitude for $O_3(\nu_3)$ and $NO(\Delta\nu = 1)$ bands for daytime and nighttime conditions and an observer at 900 km altitude. The horizontal atmospheric temperature correlation lengths of the NSS input model are also plotted for comparison.

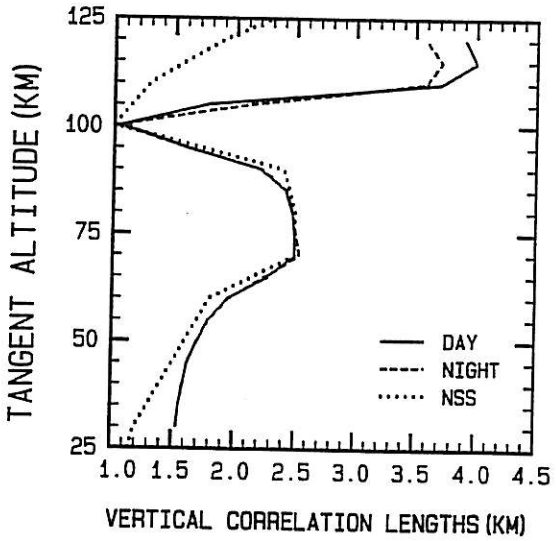

Figure 13. Vertical radiance correlation lengths plotted as a function of LOS tangent altitude for the $O_3(\nu_3)$ and $NO(\Delta\nu=1)$ bands for daytime and nighttime conditions and an observer at 900 km altitude. The vertical atmospheric temperature correlation lengths of the NSS input model are also plotted for comparison.

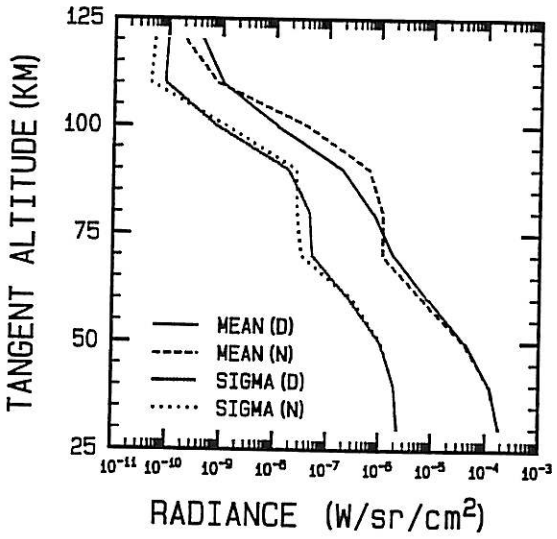

Figure 14. Mean radiances and variances of the $O_3(\nu_3)$ and $NO(\Delta\nu=1)$ bands for daytime and nighttime conditions as a function of tangent point altitude.

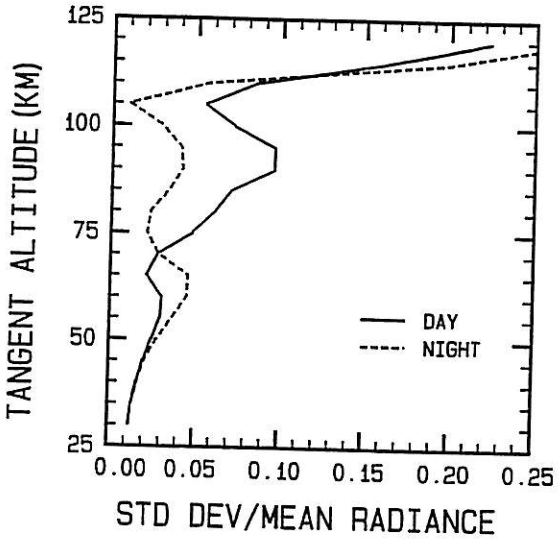

Figure 15. Relative variances of the $O_3(\nu_3)$ and $NO(\Delta\nu=1)$ band for daytime and nighttime conditions.

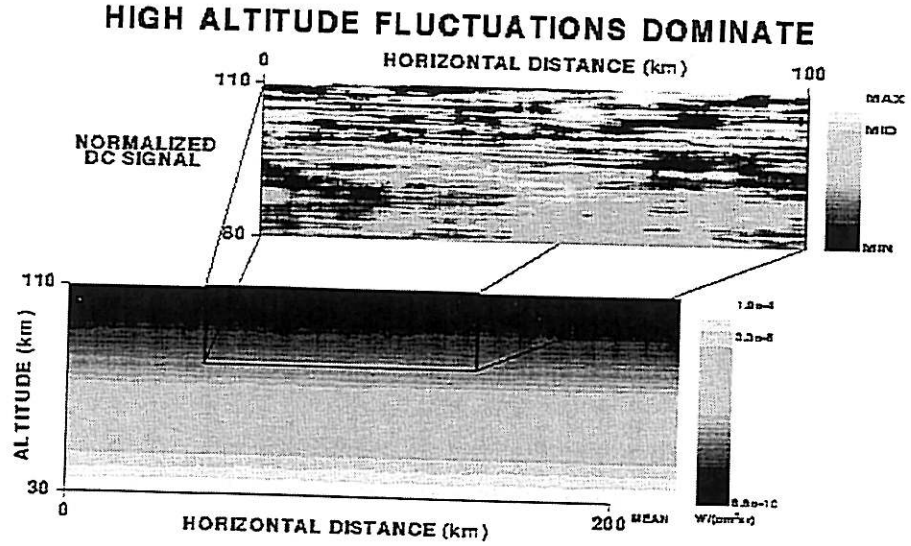

Figure 16. Image of radiance structure in the $O_3(\nu_3)$ and $NO(\Delta\nu=1)$ bands for daytime conditions.